JOURNAL OF SPACECRAFT AND ROCKETS
Vol. 32, No. 5, September–October 1995

Interactions Between Shock Wave and Hypersonic Laminar Boundary Layer Near Convex Corner

R. J. Hawboldt,* P. A. Sullivan,† and J. J. Gottlieb‡
University of Toronto, Toronto, Ontario M3H 5T6, Canada

A hypersonic gun tunnel was used to investigate a Mach 8 laminar boundary layer interacting with an externally generated shock wave impinging in the neighborhood of a convex corner. Surface static pressure measurements and schlieren photographs were taken from planar models with corner angles of 5 and 10 deg; the shock generator was set to the same angles. The results are compared with data obtained in the same tunnel for an externally generated shock impinging on a flat-plate boundary layer, and for a boundary layer interacting with a corner-expansion wave. When separation and reattachment both occur either upstream or downstream of the corner, the 5- and 10-deg interactions have similar properties; however, they differ markedly when separation is upstream and reattachment is downstream. The results also suggest that a convex corner will not completely suppress separation caused by an externally generated shock, even when impingement is close to the corner. However, the extent of separation is minimized when the separation point is located at the corner, corresponding to shock impingement 2–4 boundary-layer thicknesses downstream of the corner. Nevertheless, the overall interaction length still extends over many boundary-layer thicknesses.

Nomenclature

C	= Chapman–Rubesin constant, $\rho_e\mu_e/\rho_w\mu_w$
C_f	= skin-friction coefficient
L	= dimensionless plateau length (using free-interaction scale)
L'	= dimensionless plateau length (using δ_0)
l	= plateau length, mm
M	= Mach number
P	= free-interaction pressure scaling
p	= static pressure measured at model surface, kPa
Re	= Reynolds number based on x_{LE} and conditions behind oblique shock corresponding to α
S	= dimensionless separation length, s/l_{FP}
s	= separation length, mm
T	= temperature, K
t	= time, s
t_R	= nominal tunnel operating interval, s
X	= free-interaction length scale
x	= distance from convex corner (positive in downstream direction), mm
x_{LE}	= distance from leading edge, mm; $x = x_{\mathrm{LE}} - x_{\mathrm{LE}c}$
α	= inclination relative to freestream of plate upstream of corner, deg
γ	= specific heat ratio of gas
δ	= boundary-layer thickness, mm
θ_g	= effective flow turning angle of external shock, deg
θ_c	= convex corner angle, deg
μ	= dynamic viscosity of gas, Ns/m^2
ρ	= gas density, kg/m^3
σ	= standard deviation of unsteadiness in p/p_{FP} during t_R
Φ	= constant in Eq. (2)
χ	= viscous interaction parameter, $M_{\mathrm{FP}}^3\sqrt{(C/Re)}$

Subscripts

c	= at convex corner
d	= downstream of the interaction
e	= at edge of the boundary layer
FP	= flat plate
I	= at shock impingement point
p	= freestream pitot conditions
pe	= at end of the plateau region
pl	= plateau
r	= reattachment
s	= separation
T	= stagnation value (in tunnel reservoir)
w	= wall
Δ	= time delay between reservoir and test-section processes
∞	= tunnel freestream value
0	= beginning of the interaction

Introduction

AIR-BREATHING hypersonic propulsion systems will involve inlets in which a boundary layer develops on a long external compression surface, after which a cowl-generated oblique shock wave turns it around a convex corner into the engine. Ideally, this shock is canceled at the corner; but boundary layers cannot sustain large adverse pressure gradients, so that separation is possible. Even without separation, the interaction between a hypersonic boundary layer and an incident shock or a corner-expansion wave can extend over many boundary-layer thicknesses, thus modifying the effective corner geometry. While interactions between shock waves and boundary layers have been the subject of extensive experimental and theoretical studies in both the laminar and turbulent flow regimes,[1,2] this work has examined geometries such as a concave corner, forward- and backward-facing steps, and a flat plate with an externally generated impinging shock. We describe here an experimental investigation of the combined effect of an externally generated shock wave and a convex corner on a hypersonic laminar boundary layer. Our objective is to compare the onset and extent of separation with that of a flat-plate boundary-layer interaction.

Little has been published on the effect of an expansion corner on a shock-wave–boundary-layer interaction. In 1979, Chew[3] reported experiments at $M_\infty = 2.5$ for an adiabatic turbulent boundary layer flowing over a convex corner having $\theta_c = 6$ deg with impinging shock turning angles $\theta_g = 4$, 6, and 8 deg. The shock impingement point x_I was moved from well upstream to well downstream of the corner. Recently, Chung and Lu[4] examined the response of Mach 8 turbulent-boundary-layer interactions to an externally generated shock impinging within one boundary-layer thickness δ_0 upstream

Presented as Paper 93-2980 at the AIAA 24th Fluid Dynamics Conference, Orlando, FL, July 6–9, 1993; received March 11, 1994; revision received June 22, 1995; accepted for publication July 3, 1995.

*Research Assistant, Institute for Aerospace Studies; currently at Atomic Energy of Canada Limited, Saskatoon S7K 2C3, Canada.

†Professor, Institute for Aerospace Studies.

‡Professor, Institute for Aerospace Studies. Senior Member AIAA.

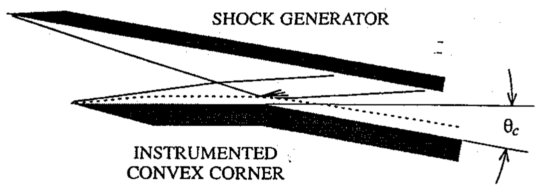

Fig. 1 Configuration of model used in tests. The angle θ_g is the turning angle of the shock-generator wave at the point of impingement on the flat-plate–expansion-corner flow.

and downstream of a convex corner. The range of these experiments was insufficient to observe the relationship between the interaction length scales, the location of shock impingement with respect to the corner, and the overall pressure rise across the interaction. Dolling and Ginoux[5] investigated a related geometry: a circular-arc expansion ramp immediately downstream of a concave corner. Their results, which included both momentum-integral predictions for a range of M_∞ and experiments at $M_\infty = 5.5$, showed that the ramp radius significantly affected both the magnitude of the pressure rise through reattachment and the overall length of the interaction.

The present experiments used a hypersonic gun tunnel,[6] which generates open-jet, Mach 8.3 flows with run times ranging from 8 to 40 ms. The model used in the tests is depicted in Fig. 1. A laminar boundary layer develops on a flat plate, and this flow then interacts with corners having $\theta_c = 5.1$ and 10.0 deg. An oblique shock is generated by an inclined flat plate located above the corner; it is mounted so that θ_g is as close as possible to θ_c, and so that x_I can be moved relative to the corner.

Experiments on interactions in gun tunnels and similar facilities encounter a number of well-known problems. These include the choice of instrumentation to reliably detect the onset and extent of separation, premature transition of boundary layers, and edge effects associated with the use of planar models. In relation to the first problem, surface static pressure measurements are the easiest to obtain reliably in such facilities, but they reveal nothing about the flow away from the model surface; furthermore, the separation and reattachment points can be difficult to locate.[2] However, when schlieren photography is combined with surface static pressure measurements, much can be learned about the overall flowfield, and the interaction length scales can be determined. This approach is adopted here, with the free-interaction concept[7] employed to assist in locating the separation point.

Data obtained previously in a gun tunnel having operating conditions close to those of the present facility[8] indicated that, at the lowest test-section Reynolds number Re attainable, the interactions should be laminar but close to transition. The onset of boundary-layer transition significantly affects the interaction between a shock wave and a boundary layer; furthermore, the disturbance of the shock may itself be sufficient to cause transition. If the flow is separated and transition occurs between separation and reattachment, the length of the interaction is reduced and the pressure gradient through reattachment is increased.[8,9] However, the pressure rise through separation is not affected by transition until the latter occurs near the separation point.[10,11] An additional complication is that noise radiated by the tunnel's nozzle boundary layer can reduce the transition Re substantially below that corresponding to free flight.[12] Therefore the onset of transition can depend on the peculiarities of a given facility, with smaller tunnels tending to be noisier. Furthermore, instabilities similar to Taylor–Görtler vortices can develop in the reattachment region of separated boundary layers. These instabilities have been attributed to irregularities in the model leading-edge thickness.[13,14] In particular, sharp leading edges necessarily have some variation in thickness and are thus more likely to produce this type of disturbance.

In view of these questions, the program finally adopted proceeded in two phases. In the first phase, exploratory models were built to facilitate design of the static-pressure-tap geometry, and to permit a preliminary investigation of transitional and model edge effects. A refined model was then built to obtain the more detailed data presented here. Data obtained from both flat-plate interactions and convex-corner-expansion flows are used to help interpret the results.

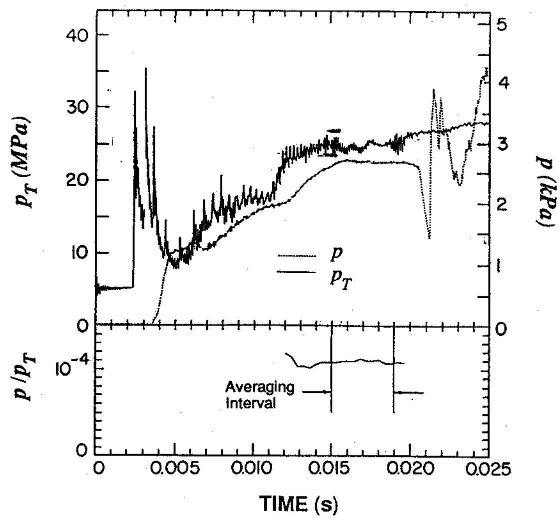

Fig. 2 Stagnation and static pressure histories for a typical experiment.

Experimental Program

Tunnel Conditions, Model, and Instrumentation

Figure 2 shows typical histories of the tunnel reservoir pressure $p_T(t)$ and a static pressure $p(t)$ recorded on the model used in the present tests. This illustrates that considerable variation in p_T can occur during the nominal operating interval t_R, which, in Fig. 2, is between 15 and 19 ms after the data acquisition system is triggered. However, p_T averaged over t_R is repeatable from run to run, being 24 ± 1 MPa for the present tests. We infer from both approximate calculations based on p_T histories[6] and a numerical simulation of the tunnel operation[15] that the mean stagnation temperature $T_T = 1300 \pm 50$ K.

Test-section pitot pressure histories $p_p(t)$ replicate closely the details of the unsteadiness in $p_T(t)$. Moreover, by aligning corresponding features of the two records to determine a time delay t_Δ associated with the propagation time from reservoir to test section, we find that the ratio $p_p(t + t_\Delta)/p_T(t)$ remains virtually constant during t_R; typically, for one tunnel run at $T_T = 1150$ K, a linear fit to this ratio showed an overall increase of 2.1% during t_R, with local fluctuations about this fit corresponding to a standard deviation of 0.8%. This and similar observations suggest that the flow generated in the test section may be assumed quasisteady. Furthermore, when averaged over t_R, p_p/p_T is repeatable from run to run; typically a sequence of 18 runs for $T_T = 950$ K gave a standard deviation of 0.81%. This quasisteadiness and repeatability played a key role in the present investigation; a pressure survey of any given configuration required several tunnel runs, and unsteadiness inherent in the phenomena being investigated could be distinguished from that associated with tunnel processes.

The numerical simulation[15] of the tunnel operation included nonequilibrium vibration and dissociation phenomena in air; it predicts that, owing to vibrational freezing of the nitrogen molecules, the flow in the tunnel nozzle may be taken as calorically perfect with $\gamma = 1.4$. Based on this assumption, we estimate M_∞ to be 8.3 ± 0.05, and the corresponding unit $Re = 20 \times 10^6$ m^{-1}. The inviscid-core diameter is about 140 mm.

The refined convex-corner model was formed by connecting two flat-plate sections to either side of a corner block. It was 133 mm wide, with 73 mm from the sharp leading edge to the convex corner, and 188 mm from the corner to the trailing edge. The static pressure taps were 0.81 mm in diameter, spaced 2.38 mm apart in the corner region and 4.76 mm near the leading and trailing edges. They were located 2.38 mm on each side of the centerline. The section upstream of the corner was inclined at $\alpha = 1.3 \pm 0.05$ deg to the freestream, so that the effective Mach number downstream of the bow shock is $M_{FP} = 8.0$; the unit $Re = 21 \times 10^6$ m^{-1}. The shock generator was adjusted so that θ_g was within 0.1 deg of θ_c.

Static pressures were measured with a variety of piezoresistive pressure transducers with ranges from 30 to 100 kPa. The output signals were conditioned and amplified by proprietary signal

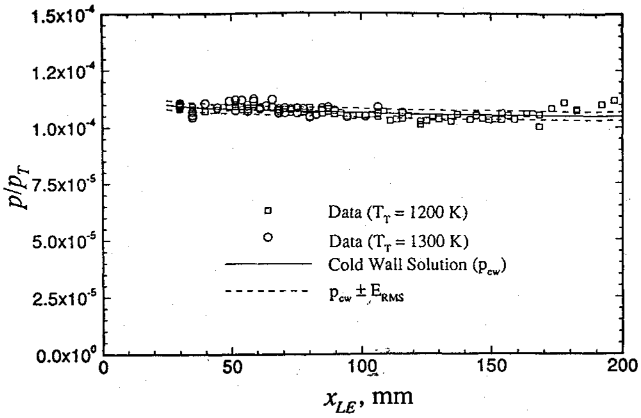

Fig. 3 Measured pressure distribution on the flat plate compared with predictions of the theory of Ref. 16 for viscous–inviscid interaction extending from the leading edge. The quantity E_{RMS} is the root-mean-square deviation of the measurements about the theory.

conditioners and filtered at a cutoff frequency of 20 kHz. The history of p_T was measured at the end of the gun-tunnel compression tube with a piezoelectric pressure transducer. All pressure histories were recorded digitally at 250 kHz. The combined measurement uncertainty of p/p_T, including the pressure transducers, signal conditioners, and data acquisition system, was ±2%.

The schlieren system employed a modified camera flash as its light source. The flash duration was about 250 μs, or about the time required for a fluid particle to travel about 1.5 model chords. Because the tunnel freestream had high-frequency unsteadiness, the resulting photograph was thus a time-averaged record of the flowfield.

Interpretation of Pressure Histories

All static pressures measured on the model were normalized using the procedure adopted for pitot pressures. An example is given in Fig. 2; as can be seen, $p(t+t_\Delta)/p_T(t)$ is effectively constant. As a test of the reliability of this procedure, with the shock generator removed, the flat-plate model was inclined to the flow at $\alpha = 1.3$ deg and the surface pressures were measured. They were then compared with predictions of an approximate theory of Sullivan[16] for the viscous–inviscid interaction extending from the leading edge. This theory is based on the cold-wall similarity concept for the boundary layer and the tangent-wedge rule for inviscid flow. The results are presented in Fig. 3; p was measured at certain locations on the plate as many as 10 times. The root-mean-square deviation of the measurements about Sullivan's solution is 1.8%. Notwithstanding the repeatability implied by these results, as a control in subsequent experiments, pressure measurements were repeated from run to run for at least one station on the model, with additional repetitions being made in high-gradient regions.

Schlieren photographs were analyzed using an optical comparator; this enabled model angles to be measured to within ±0.01 deg, and shock angles to within ±0.25 deg. Estimates of shock angles were further refined to an accuracy of ±0.1 deg by using measured pressure jumps in conjunction with the standard oblique shock formulas. The photographs, in conjunction with the static pressure distributions, were also used to locate the major features of separated regions, such as the shock impingement point and separation point.

Effects of Boundary-Layer Transition

In investigating boundary-layer phenomena close to transition, if the experimental results for models with slight configuration changes are to be compared, it seems prudent to replicate as closely as possible as many parameters that influence transition. These include $Re_0 = Re(x_{LE0})$, the model leading-edge bluntness, and the wall temperature, as well as the orientation and position of the model with respect to the wind-tunnel nozzle. Since there was a large variation in x_I, Re_0 varied by a factor of 2. Also, in order to minimize entropy-layer effects, the leading edge was sharpened as much as possible, even though this increased the possibility of boundary-layer instabilities developing during reattachment.[14]

It is not possible to reliably detect the onset of boundary-layer transition using surface static pressure measurements and schlieren flow visualization.[9] However, surface-flow visualization combined with static pressure history measurements[17] on one exploratory model showed that, when transition began near separation, the separation point oscillated or moved downstream during t_R. Therefore the interactions were located as close as possible to the model leading edge in order to minimize Re_0, and thus to prevent transition from affecting the flow near the free-interaction region. In most cases this was accomplished.

Model Edge Effects

Tests for model edge effects focused on two aspects: disturbances created by the instrumentation housing and supporting system on the model underside, and leakage from separated regions into the freestream. These tests used two exploratory models to determine a suitable width.[17] The first was a flat plate having pressure taps across its span at $x_{LE} = 102$ and 203 mm. For this model $\alpha = 4$ deg, so that p/p_∞ was about 2.2, close to the plateau pressure in the study. As the plate width was reduced from 152 to 114 mm, at $x_{LE} = 102$ mm the influence of the edge on the spanwise pressure distribution extended inward 25 mm from the model edges, with the rest of the distribution remaining constant and equal to the centerline value. The second exploratory model consisted of a 10.0-deg convex corner with a 10.0-deg shock generator located so that a large separated region was generated upstream of the corner. The width of this model was reduced in steps from 127 to 76 mm. Both the centerline pressure distribution through the entire interaction and the interaction length remained constant until the width was 76 mm, and then the extent of separation decreased significantly. This decrease was the only significant difference in the pressure distribution, indicating that it was the most sensitive indicator of the presence of edge effects and that the present model width of 133 mm was adequate. To eliminate the effects of disturbances created by model supports and instrumentation, the refined model included 51-mm skirts extending towards its underside.

Interaction Length Scales

To quantify the effect of the convex corner on the interaction, we determined the effect of the shock impingement position relative to the corner x_I on a suitable measure of the interaction length, and then compared this length with its equivalent for a flat-plate interaction. The important features of a flat-plate interaction are depicted in Fig. 4. We chose the distance between the separation point and the end of the pressure plateau, the plateau length l depicted in Fig. 4, as the interaction length scale, because, using the procedure

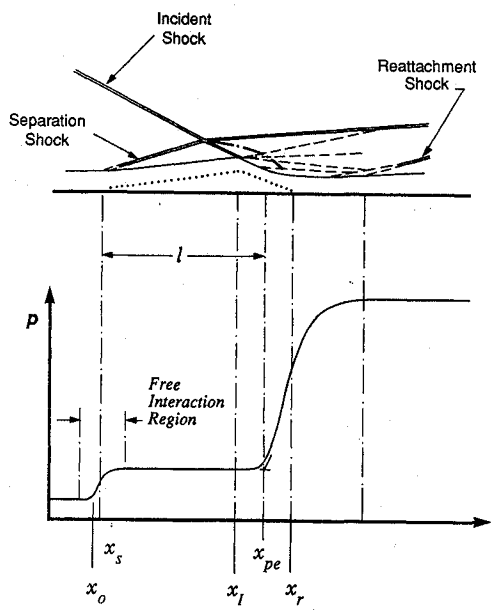

Fig. 4 Sketch of an incident shock interacting with a flat-plate hypersonic boundary layer.

outlined below, in most cases it could be readily measured to within ± 1 mm. The separation length s—the distance between the separation and reattachment points—was also estimated. However, because it is difficult to locate reattachment precisely using pressure measurements,[11] we consider s to be a less reliable measure of the interaction length.

Separation points x_s were located using the static pressure data in conjunction with schlieren photographs and, whenever possible, using the free-interaction concept. According to this concept, both the pressure distribution through the free-interaction region and the location of separation depend only on the state of the approaching boundary layer, and not on the mechanism causing separation. Furthermore, they can be predicted by a semiempirical correlation[18] using suitable scaled coordinates.[7,9,19] The pressure coordinate is[7,19]

$$P = \frac{2(p - p_0)}{\gamma M_0^2 p_0} \frac{\left(M_0^2 - 1\right)^{\frac{1}{4}}}{\sqrt{C_{f0}}} \tag{1}$$

and the length coordinate for a nonadiabatic wall is, according to Curle,[19]

$$X = \Phi \frac{x_{\mathrm{LE}} - x_{\mathrm{LE0}}}{x_{\mathrm{LE0}}} \frac{M_0^2}{\sqrt{\chi_0}} \frac{T_0}{T_w} \tag{2}$$

Katzer[20] noted that, depending on the analysis technique used, the reported value of P in Eq. (1) corresponding to separation, P_s, ranges from 1.15 to 1.45. We chose $P_s = 1.25$; for the range of P_s given by Katzer, and for the flow conditions considered here, the corresponding uncertainty in x_s is ± 0.5 mm. The constant Φ in Eq. (2) was determined by using the procedures suggested in Ref. 11.

The end of the plateau, x_{pe}, was located by visually fitting straight lines to the pressure distributions in the plateau region and to the steepest part of the reattachment region. Then, as shown in Fig. 4, x_{pe} is defined as the intersection of these lines. To estimate a nominal x_r, following suggestions discussed by Charwat,[11] we assumed that reattachment occurs at 50% of the pressure rise between the plateau and the maximum pressures. However, as Charwat notes, this approach cannot be considered to be as reliable as its equivalent for separation in a free interaction, especially for the present configuration. Finally, $l = x_{\mathrm{pe}} - x_s$ and $s = x_r - x_s$.

Because the length of the interaction depends on the state of the boundary layer immediately upstream, to make the comparisons attempted here, one should ideally keep x_{LE0} the same for all cases. For the present tests this was not feasible; x_{LE0} varied by a factor of 2. Furthermore, as the results in Fig. 3 show, the effect of leading-edge viscous–inviscid interaction could not be completely neglected. To compensate for the latter effect, the measured p/p_T distribution through each interaction was normalized by the pressure distribution on a flat plate predicted by Sullivan's theory.[16] To compensate for the effect of variation in x_{LE0}, we note that, while the validity of the scaling in the free-interaction region has been verified, no corresponding consensus exists for the overall interaction length scale.[20] Therefore, to facilitate comparison of the measured l with its flat-plate equivalent for such a large variation in x_{LE0}, l was nondimensionalized in two ways: the first used δ_0, and the second used Eq. (2).

We consider δ_0 suitable because many of the factors that affect the interaction length also affect δ_0 in a qualitatively similar manner. However, it could not be accurately measured in the present experiments; hence it was estimated using Sullivan's solution[16] in conjunction with schlieren photographs. For interactions occurring downstream of the corner, by using the measured value of p_0 rather than x_{LE0}, δ_0 was determined from Sullivan's solution, which includes the effect of the corner-expansion wave. The resulting nondimensional plateau length is $L' = l/\delta_0$.

In using Eq. (2), we replace $x_{\mathrm{LE}} - x_{\mathrm{LE0}}$ with the plateau length l, giving the nondimensional plateau length L. Like δ_0, it characterizes the incoming flat-plate boundary layer; furthermore, it can be determined from the data collected in the experiments more accurately than can δ_0. When the interaction begins downstream of the convex corner, the values of M_0 and χ_0 correspond to the flat-plate boundary-layer conditions at the same x_{LE0}. This procedure simplifies comparison because it eliminates the need for detailed knowledge of the accelerating boundary layer in the immediate region of the corner. However, the free-interaction length scale cannot be assumed applicable when the interaction begins downstream of the corner.

To facilitate comparison with the flat-plate results, L and L' were normalized by the flat-plate equivalents, L_{FP} and L'_{FP}, resulting from the same θ_g. This procedure clearly reveals the effect of the proximity of the convex corner to the interaction. Furthermore, the data were presented in this form because it compensates for two potential sources of error. The first stems from any arbitrariness in the methods used to determine l, such as that associated with the choice of constants in Eqs. (1) and (2). The second arises from possible transitional effects downstream of separation in reducing l.

Results

Representative results for the three model geometries are presented in the following. In each case, measured surface static pressure distributions are plotted below schlieren photographs that are scaled and aligned with the abscissa. The flow is from left to right in these figures. Whenever possible, the static pressure distribution near separation predicted by the free-interaction concept is also plotted, with a vertical line indicating the estimated separation-point location.

Flat-Plate Interactions

With the shock generator positioned so that the incident shock wave impinged at $x_{\mathrm{LE}} \approx 73$ mm, θ_g was set at 2.6, 5.1, 7.4, and 10.0 deg; both pressure distributions and schlieren photographs showed that separation occurred for the last three cases. The results for $\theta_g = 5.1$ and 10.0 deg are shown in Fig. 5. The horizontal lines on the right side of the plot mark the pressure ratio p_d/p_0 corresponding to an ideal reflection of an incident shock. The two points for $\theta_g = 5.1$ deg in the reattachment region at $x_{\mathrm{LE}} = 83$ mm provide a good indication of the distinction that could be made between the unsteadiness associated with variations in p_T and that inherent in the flow. For two successive runs, when averaged over t_R, p/p_T differed by about 2.3%. However, significant oscillations in p/p_T about the average occurred. A standard deviation σ for these oscillations during t_R was computed, and bars indicating $\pm 3\sigma$ are marked on the record, indicating, in this case, an oscillation of about $\pm 5.5\%$. Bars marking $\pm 3\sigma$ are indicated at selected locations on all the distributions.

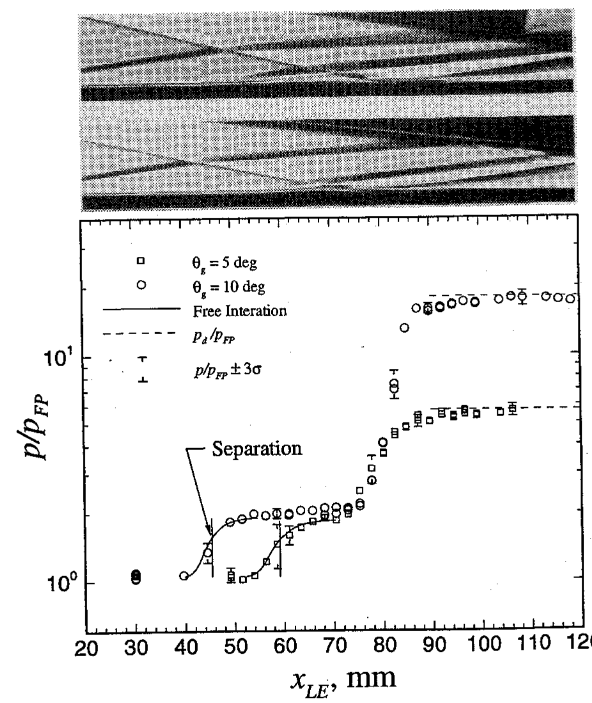

Fig. 5 Static pressure distributions through two flat-plate interactions: $\theta_g = 5.1$ and 10.0 deg.

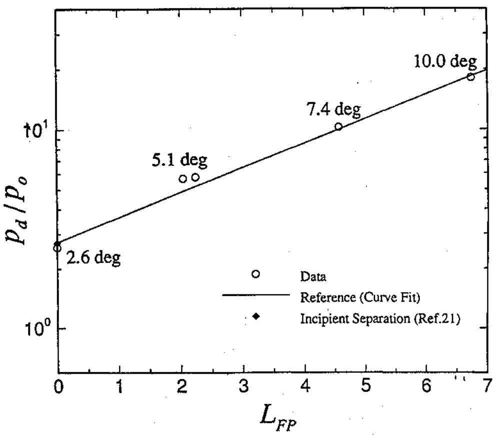

Fig. 6 Relationship between the overall pressure ratio across the flat-plate interaction and the nondimensional plateau length. As L_{FP} increases from zero, the data correspond, respectively, to θ_g = 2.6, 5.1 (two points), 7.4, and 10.0 deg.

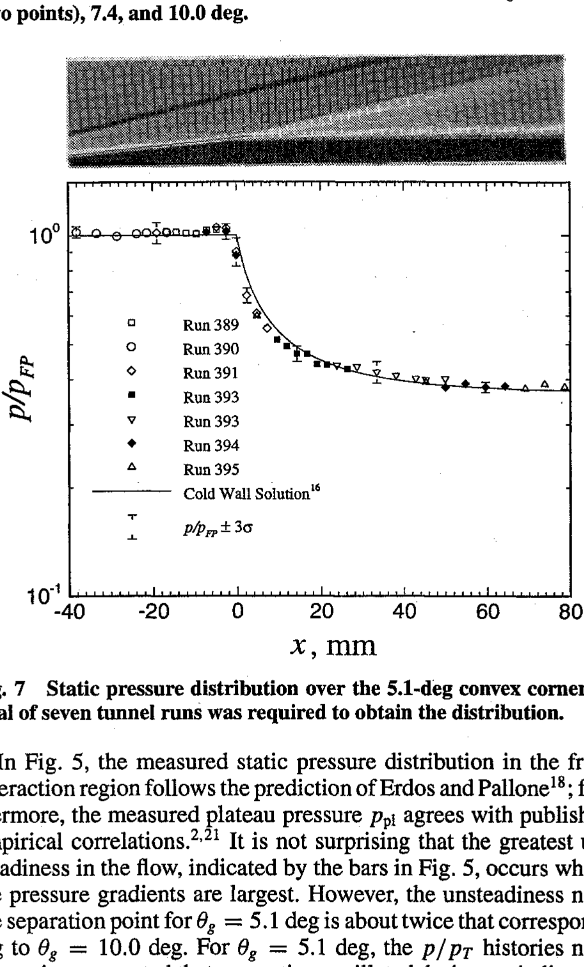

Fig. 7 Static pressure distribution over the 5.1-deg convex corner. A total of seven tunnel runs was required to obtain the distribution.

In Fig. 5, the measured static pressure distribution in the free-interaction region follows the prediction of Erdos and Pallone[18]; furthermore, the measured plateau pressure p_{pl} agrees with published empirical correlations.[2,21] It is not surprising that the greatest unsteadiness in the flow, indicated by the bars in Fig. 5, occurs where the pressure gradients are largest. However, the unsteadiness near the separation point for $\theta_g = 5.1$ deg is about twice that corresponding to $\theta_g = 10.0$ deg. For $\theta_g = 5.1$ deg, the p/p_T histories near separation suggested that separation oscillated during t_R, indicating the presence of transition near reattachment.

For this flat-plate interaction, as θ_g increases, both l_{FP} and s_{FP} increase; L_{FP} is plotted versus p_d/p_0 in Fig. 6. The value of p_d/p_0 corresponding to incipient separation, as determined by an empirical correlation reported by Stollery,[21] is indicated in this plot. For the subsequent data reductions, the relationship between L_{FP} and p_d/p_0 was estimated by fitting a straight line through Stollery's incipient-separation estimate and the data in Fig. 5 for $\theta_g = 7.4$ and 10.0 deg; the data for $\theta_g = 5.1$ deg were excluded because we believe l_{FP} was decreased slightly by transition. Note that Stollery's estimate[21] implies that incipient separation should occur for θ_g close to 2.6 deg; this is consistent with the present results.

Corner-Expansion Flows

With the shock generator removed, the pressure decay immediately downstream of the corner was measured. Figure 7 compares the measured pressure distribution for $\theta_c = 5.0$ deg with Sullivan's prediction.[16] As a second demonstration of the repeatability of our experiments, data from individual tunnel runs are identified. Furthermore, the agreement with the theory, together with this repeatability, provide additional evidence of the validity of the data reduction procedures used here. The minimal upstream influence and very long wall-static-pressure decay downstream of the corner, typical of hypersonic corner expansions,[22] are clearly shown in this figure. Sullivan's solution cannot predict the pressure relief that occurs upstream of the corner in hypersonic flows, so that the displacement of the data from that solution is a measure of this relief.

The upstream section of the convex-corner models had the same position and orientation as the flat-plate model, so that the static pressure downstream of the convex corner was far below p_∞. As a result, the flow at the downstream end of the 10.0-deg model was disrupted, either by flow around the edges or by separation at the downstream end, or by both. However, the flow near the convex corner and over the entire length of the 5.1-deg model was free of these effects.

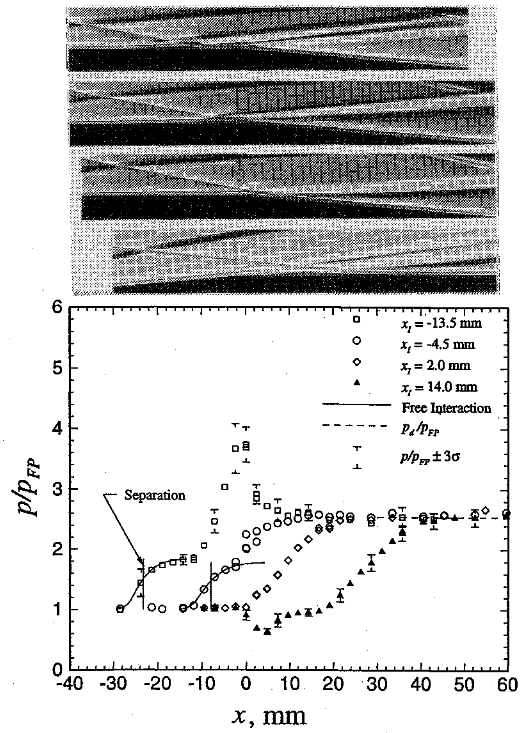

Fig. 8 Static pressure distributions through four interactions near the 5.1-deg convex corner.

Convex-Corner Interactions

Samples of the results for cases when the boundary layer was influenced by both an incident shock wave and the convex corner are given in Figs. 8–10. For $\theta_c = 5.0$ deg, we have $\theta_g = 5.1$ deg and $-19\delta_c \le x_I \le 25\delta_c$. Here δ_c is the boundary-layer thickness at the corner in the absence of an external shock; using Sullivan's theory[16] in conjunction with the schlieren photographs, we estimate it to be 0.7 mm. The ideal p_d/p_0 corresponding to shock impingement at the corner is 2.54 and is indicated by a dashed line in Fig. 8. For $\theta_c = 10$ deg, we have $\theta_g = 9.9$ deg, giving $p_d/p_0 = 5.06$ and $-14\delta_c \le x_I \le 43\delta_c$. The peak pressures in Figs. 8 and 9, for $x_I = -13.5$ and -10.5 mm, respectively, are substantially below the values of p_d for the corresponding flat-plate interactions, indicating that for negative x_I we were unable to completely uncouple the separation and corner-expansion processes. This was also the case for $x_I > 0$.

When the shock impinges well upstream or well downstream of the corner, the interactions resemble those observed on the flat-plate boundary layer. For interactions occurring upstream of the corner, the boundary layer separates well upstream of x_I, and a pressure plateau is formed. The pressure rises through reattachment

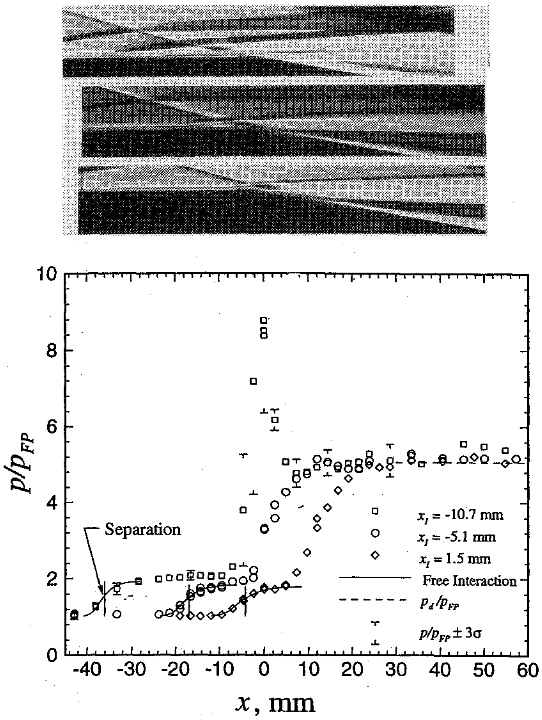

Fig. 9 Static pressure distributions through three interactions beginning upstream of the 10.0-deg convex corner.

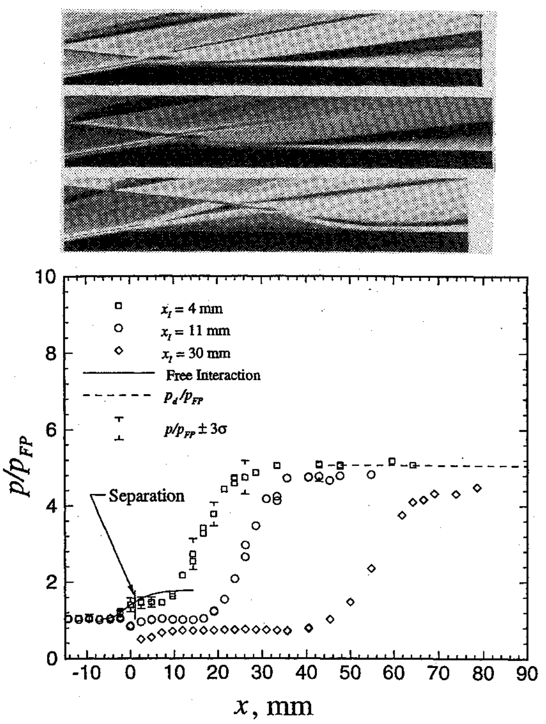

Fig. 10 Static pressure distributions through three interactions beginning near or downstream of the 10.0-deg convex corner.

to a maximum before undergoing a fluctuating decay to the ideal value. By fitting straight lines through the data corresponding to the increasing pressure upstream of the corner and to the decreasing pressure downstream, the location of the maximum pressure is estimated to be approximately $1.5\delta_c$ upstream of the corner. The fluctuation in pressure just downstream of the corner is believed to be caused by the intense interaction of the reattachment compression and the corner expansion with the thin boundary layer. Finally, the data in Figs. 8 and 9 show that, when separation occurs upstream of the corner, the pressure rise to the plateau value is predicted by the free-interaction concept.

When separation occurs downstream of the corner, p/p_{FP} increases from a level observed for the corner expansion to a plateau followed by a smooth, gradual rise to the ideal value, as shown in Figs. 8 and 10. The mechanism causing separation appears to be similar to that corresponding to a free interaction. That is, separation occurs well upstream of the disturbance causing it; therefore, it is unlikely to depend on the nature of the disturbance. However, we believe that the correlations to predict the rise in pressure to the plateau are inapplicable owing to the distorted velocity profiles of the accelerating boundary layer near the corner. As a result of both the extended l and gradual rise of p from p_{pl} to p_d, the overall interaction becomes very long. For example, in Fig. 10, the entire interaction for $x_I = 30$ mm ($43\delta_c$) extends over $130\delta_c$.

When the shock impinges near the corner, the differences between the results for the two values of θ_g are more marked. As shown by the static pressure data and the schlieren photograph in Fig. 8 for $\theta_c = 5.1$ deg, separation is nearly eliminated when $x_I = 2$ mm. In contrast, for $\theta_c = 10.0$ deg, the data in Figs. 9 and 10 show that an identifiable separation region exists for all x_I.

Discussion

Presented below are the effects of the shock impingement position with respect to the corner on the extent of boundary-layer separation. Figures 11 and 12 give x_s, x_{pe}, and x_r as a function of x_I for the two θ_c. Figures 13 and 14 plot L/L_{FP}, L'/L'_{FP}, and S against x_I/l_{FP}. The results show that, for both configurations, the plateau length is at a minimum when the shock impinges near the corner. However, it is useful to consider each θ_c separately, and to identify three interaction cases. These are 1) both separation and reattachment occur upstream of the corner, 2) separation occurs either upstream or at the corner, and reattachment occurs downstream, and 3) separation and reattachment both occur downstream of the corner.

Separation and Reattachment Occur Upstream of Corner

If x_I is located far enough upstream from the corner, a standard flat-plate interaction should be distinguishable and separated from the convex-corner expansion. However, for $x_I = -13.5$ mm in Fig. 8

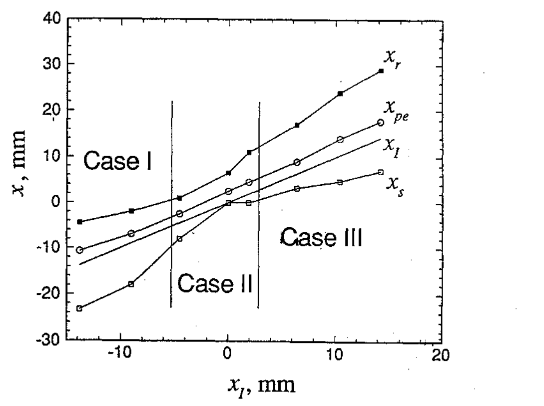

Fig. 11 Location of x_s, x_{pe}, and x_r with respect to x_I for $\theta_g = 5$ deg.

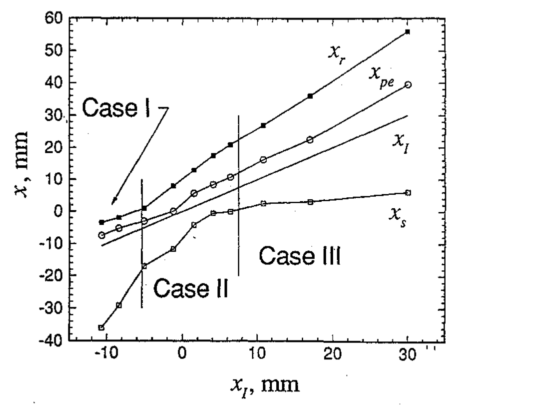

Fig. 12 Location of x_s, x_{pe}, and x_r with respect to x_I for $\theta_g = 10$ deg.

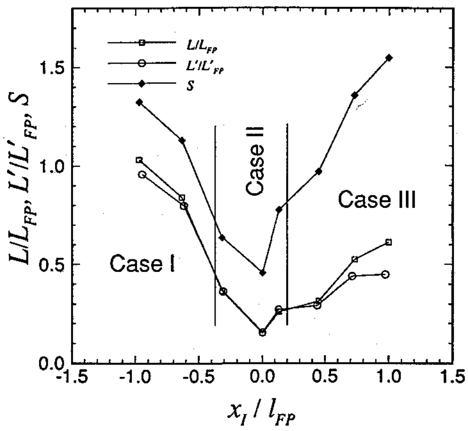

Fig. 13 Comparison of $L/L_{\rm FP}$, $L'/L'_{\rm FP}$, and S for θ_c = 5.1 deg.

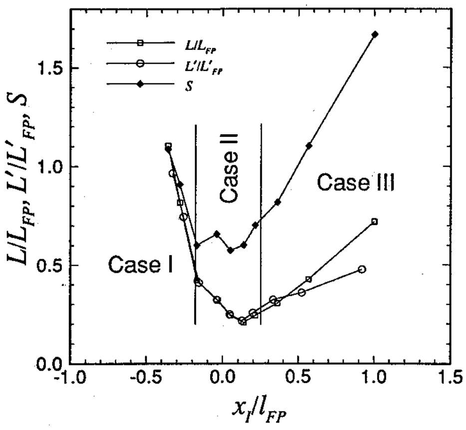

Fig. 14 Comparison of $L/L_{\rm FP}$, $L'/L'_{\rm FP}$, and S for θ_c = 10.0 deg.

and for $x_I = -10.7$ mm in Fig. 9, the static pressure never reaches the value expected downstream of a flat-plate interaction, so that we were unable to completely decouple the two processes. As x_I and x_r move closer to the corner, $L/L_{\rm FP}$ decreases rapidly for both configurations, but x_s remains well upstream of x_I, and the free-interaction concept accurately predicts the pressure through the separation region. This indicates that the separation process is unaffected by the proximity of the corner. The decrease in l and s observed as x_I approaches the corner results from the changing conditions near reattachment. Because some pressure relief is provided by the corner expansion, the adverse pressure gradient near reattachment is reduced, and l and s also decrease. This is analogous to reducing θ_g in the flat-plate interaction. By graphically interpolating the data in Figs. 11–14, we estimate that the reattachment point reaches the corner when $x_I/l_{\rm FP} = -0.32$ ($x_I = 4.5$ mm) for $\theta_c = 5.1$ deg, and $x_I/l_{\rm FP} = -0.17$ ($x_I = 5.1$ mm) for $\theta_c = 10.0$ deg.

Separation Bubble Straddles the Corner

For this case the interactions for $\theta_c = 5.1$ and 10.0 deg differ markedly, so they are discussed separately. Consider first $\theta_c = 10.0$ deg; when x_r first moves downstream of the corner, corresponding to the pressure distribution for $x_I = -5$ mm in Fig. 9, the interaction is nearly unchanged. The free-interaction prediction shows that separation occurs as in a flat-plate boundary layer, so that the concept can be used to locate x_s. The recirculation bubble seems to accommodate the change in wall slope, so that the flow at the boundary-layer edge resembles that of a flat-plate interaction. However, Fig. 14 shows that $L/L_{\rm FP}$ begins to decrease much more slowly, and that S increases slightly. This discrepancy between $L/L_{\rm FP}$ and S is due primarily to the normalization procedure; the distances x_s, x_r, and x_I are measured along the model surface, but the shock impingement point is actually located at the edge of the separated boundary layer, well above the model surface.

Through interpolation of the data in Fig. 14, we estimate that the interaction length is minimized when x_s is located at the corner, or $x_I/l_{\rm FP} = 0.09$ with $x_I = 2.7$ mm. Until this condition is reached, the flat-plate free-interaction correlation appears to apply up to the separation point, as shown in Fig. 10 for $x_I = 4$ mm. As x_I moves further downstream, the end of the pressure plateau and reattachment point are also pushed downstream, but from detailed examinations of the schlieren photograph and the pressure distribution, we infer that the separation point remains close to the corner, so that l and s increase.

Whereas for $\theta_c = 10.0$ deg the separation bubble extends around the corner, Fig. 11 shows that for $\theta_c = 5.1$ deg, separation is nearly eliminated when the shock impinges near the corner. In Fig. 8 ($x_I = 2$ mm), separation is suggested by a small kink in the pressure distribution, but the schlieren photograph shows that this has very little effect on the flow above the boundary layer. Now, even when shock impingement on a flat-plate boundary layer is not strong enough to provoke separation, the resulting interaction extends[16,22] over several δ_0. In this case, the abrupt change in wall slope at the corner, and not the pressure gradient imposed by the incident shock, may be primarily responsible for the appearance of a small separation bubble. As indicated in Fig. 6, the overall pressure ratio across this interaction was slightly less than the predicted incipient separation pressure ratio for a flat-plate interaction.[21] For $\theta_c = 10.0$ deg, corresponding to a much higher p_d/p_0, we believe that the pressure gradient is primarily responsible for separation, because the change in wall slope at the corner appears to be easily accommodated by the separation bubble.

Separation and Reattachment Occur Downstream of Corner

When x_I moves far enough downstream, one would expect the interaction to again resemble that on a flat plate. There is evidence of this in Fig. 13, corresponding to $\theta_c = 5.1$ deg, in that $L'/L'_{\rm FP}$ becomes nearly constant for $x_I/l_{\rm FP} \geq 0.7$. However, corresponding behavior is not observed in Fig. 14 for $\theta_c = 10.0$ deg, indicating that the interaction length is still strongly influenced by conditions near the separation point. In a hypersonic flow over a convex corner, the wall shear stress increases sharply at the corner, and then gradually decays downstream to corresponding flat-plate values.[22,23] Therefore, because of the high wall shear stress just downstream of the corner, initiation of boundary-layer separation in this region is expected to be more difficult. In other words, as x_I decreases from far downstream, the progression of x_s upstream is blocked by the high levels of shear stress generated by the corner. Finally, we believe that when the interaction begins downstream of the corner, δ_0 is a more realistic nondimensionalization scale than Curle's variables.

Conclusions

The results show that shock-wave–laminar-boundary-layer interactions in the neighborhood of a convex corner extend over a considerable distance, so that the ideal of shock cancellation is probably not attainable. Flow separation is minimized when separation occurs at the corner, corresponding to shock impingement between $2\delta_c$ and $4\delta_c$ downstream of the corner, yet the minimum overall interaction lengths for the 5.1- and 10.0-deg configurations are $37\delta_c$ and $54\delta_c$, respectively. When separation and reattachment occur either upstream or downstream of the corner, the interactions are very similar to the flat-plate case. However, when separation occurs either upstream of or at the corner, and reattachment occurs downstream, the overall pressure ratio and the sharpness of the corner appear to affect the structure of the separation bubble. If the overall pressure ratio is large enough to provoke significant separation, the shape of the corner has little effect on the structure of the interaction. However, when the pressure ratio is near that for incipient separation, the sharpness of the corner may be important. It also appears that correlations for the prediction of incipient separation for the flat-plate interaction may be used as a guide to predict separation in interactions near a convex-corner. If the pressure ratio across the interaction is sufficient to cause separation on a flat plate, separation will apparently occur for the convex-corner case, regardless of where shock impingement occurs. Finally, the normalizations proposed here appear to provide a useful basis for quantifying the effect of a convex corner on a shock-wave–boundary-layer interaction suitable for comparison of experimental or numerical results obtained under a wide range of flow conditions.

Acknowledgments

Part of the work described here was funded by the United States Air Force and by Johns Hopkins University's Applied Physics Laboratory (JHU). The tunnel was donated to the University of Toronto Institute for Aerospace Studies (UTIAS) by the National Research Council of Canada (National Aeronautical Establishment). The Natural Sciences and Engineering Research Council of Canada provided an equipment grant for upgrading the tunnel and additional operating grants. We particularly wish to acknowledge technical advice provided by M. E. White of JHU and strong institutional support and encouragement provided by R. C. Tennyson, Director of UTIAS.

References

[1]Delery, J., and Marvin, J. G., "Shock-Wave Boundary Layer Interactions," AGARDograph AG-280, Feb. 1986.

[2]Hankey, W. L., and Holden, M. S., "Two-Dimensional Shock Wave–Boundary Layer Interactions in High Speed Flows," AGARDograph AG-203, June 1975.

[3]Chew, Y. T., "Shock Wave and Boundary Layer Interaction in the Presence of an Expansion Corner," *Aeronautical Quarterly*, Vol. 30, Pt. 3, 1979, pp. 506–527.

[4]Chung, K.-M., and Lu, F. K., "Hypersonic Turbulent Expansion–Corner Flow with Shock Impingement," AIAA Paper 92-0312, Jan. 1992.

[5]Dolling, D. S., and Ginoux, J. J., "Effect of Shock Impingement on Heat Transfer: A Futher Experimental and Theoretical Investigation of Adiabatic Laminar Boundary Layer/Shock Wave Interactions on Curved Walls," von Kármán Inst. for Fluid Dynamics, TN 115, Rhode-Saint-Genese, Belgium, Jan. 1976.

[6]Deschambault, R. L., Hawboldt, R. J., Sullivan, P. A., and Molder, S., "The University of Toronto–Ryerson Polytechnical Institute Hypersonic Gun Tunnel," *Proceedings of the First Canadian Symposium on Aerodynamics*, Canadian Aeronautics and Space Inst., Ottawa, ON, Canada, 1989, pp. 35.1–35.3.

[7]Chapman, D. R., Kuehn, D. M., and Larson, H. K., "Investigation of Separated Flows in Supersonic and Subsonic Streams with Emphasis on the Effect of Transition," NACA Rept. 1356, 1958.

[8]Needham, D. A., and Stollery, J. L., "Hypersonic Studies of Incipient Separation and Separated Flows," Aeronautical Research Council, England, UK, Rept. 27-752, Hyp. 539, Jan. 1966.

[9]Lewis, J. E., Kubota, T., and Lees, L., "Experimental Investigation of Supersonic Laminar Two-Dimensional Boundary Layer Separation in a Compression Corner With and Without Cooling," *AIAA Journal*, Vol. 6, No. 1, 1968, pp. 7–14.

[10]Ginoux, J. J., "Supersonic Separated Flows over Wedges and Flares with Emphasis on a Method of Detecting Transition," Aerospace Research Labs., Rept. ARL-69-009, Wright–Patterson AFB, Jan. 1969.

[11]Charwat, A. F., "Supersonic Flows with Imbedded Separated Regions," *Advances in Heat Transfer*, Vol. 6, edited by J. P. Harnett and J. F. Irvine Jr., Academic, New York, 1970, pp. 1–133.

[12]Arnal, D., "Laminar–Turbulent Transition Problems in Supersonic and Hypersonic Flows," *AGARD–FDP–VKI Special Course on Aerothermodynamics of Hypersonic Vehicles*, AGARD Rept. 761, May–June 1988, pp. 8.1–8.45.

[13]Ginoux, J. J., "On Some Properties of Reattaching Laminar and Transitional High Speed Flows," von Kármán Inst. for Fluid Dynamics, TN-53, Rhode-Saint-Genese, Belgium, Sept. 1969.

[14]Simeonides, G., Vermeulen, J. P., and Zemsch, S., "Amplification of Disturbances and the Promotion of Laminar–Turbulent Transition Through Regions of Hypersonic Shock Wave Boundary Layer Interaction," *Proceedings of the IUTAM Symposium on Aerothermochemistry of Spacecraft and Associated Hypersonic Flows* (Marseille, France), edited by R. Brun and A. A. Chikhaoui, Sept. 1992, pp. 344–351.

[15]Groth, C. P. T., Gottlieb, J. J., and Sullivan, P. A., "Numerical Investigation of High-Temperature Effects in the UTIAS–RPI Hypersonic Impulse Tunnel," *Canadian Journal of Physics*, Vol. 69, No. 7, 1991, pp. 897–918.

[16]Sullivan, P. A., "Interaction of a Laminar Hypersonic Boundary Layer and a Corner Expansion Wave," *AIAA Journal*, Vol. 8, No. 4, 1970, pp. 765–771.

[17]Hawboldt, R. J., "An Experimental Study of Shock Wave and Boundary Layer Interactions Near a Convex Corner," Ph.D. Thesis, Univ. of Toronto, ON, Canada, Dec. 1993.

[18]Erdos, J., and Pallone, A., "Shock/Boundary-Layer Interaction and Flow Separation," *Heat Transfer and Fluid Mechanics Institute Proceedings*, Stanford Univ. Press, Stanford, CA, 1962, pp. 239–254.

[19]Curle, N., "The Effects of Heat Transfer on Laminar-Boundary-Layer Separation in Supersonic Flow," *The Aeronautical Quarterly*, Vol. 12, Nov. 1961, pp. 309–336.

[20]Katzer, E., "On the Lengthscales of Laminar Shock/Boundary-Layer Interaction," *Journal of Fluid Mechanics*, Vol. 206, Sept. 1989, pp. 477–496.

[21]Stollery, J. L., "Viscous Interaction Effects on Re-Entry Aerothermodynamics: Theory and Experimental Results," *Aerodynamic Problems of Hypersonic Vehicles*, AGARD-LS-42-72, July 1972.

[22]Rizzetta, D. P., Burggraf, O. R., and Jenson, R., "Triple-Deck Solutions for Viscous Supersonic and Hypersonic Flow Past Corners," *Journal of Fluid Mechanics*, Vol. 89, Dec. 1978, pp. 535–552.

[23]Lo, A. K., and Sullivan, P. A., "A Complete Solution to the Viscous–Inviscid Equations for the Interaction of a Laminar Hypersonic Boundary Layer with a Corner Expansion Wave," AIAA Paper 70-807, July 1970.

J. C. Adams
Associate Editor